Site Occupancy Determination in Th 2 Zn 17 - and TbCu 7 -types Sm 2 Fe 17− x Co x Compounds using Synchrotron Resonant Diffraction

Thomas Bartoli, Jean-Marc Joubert, Karine Provost, Erik Elkaim, Valérie Paul-boncour, Judith Monnier, Jacques Moscovici, Lotfi Bessais

Site occupancy determination in Th_2Zn_{17}- and $TbCu_7$-types $Sm_2Fe_{17-x}Co_x$ compounds using synchrotron resonant diffraction

Thomas Bartoli[1], Jean-Marc Joubert[1,*], Karine Provost[1], Eric Elkaim[2], Valérie Paul-Boncour[1], Judith Monnier[1], Jacques Moscovici[1], Lotfi Bessais[1]

[1] Univ Paris Est Créteil, CNRS, ICMPE, UMR 7182, 2 rue Henri Dunant, 94320 Thiais, France

[2] SOLEIL, L'Orme des Merisiers, Saint-Aubin, BP 48, 91192 Gif-sur-Yvette Cedex, France

[*] Corresponding author: joubert@icmpe.cnrs.fr, phone: +33 1 49 78 13 44

Abstract

Sm_2Fe_{17} compounds are high performance permanent magnets. Cobalt substitution allows to further improve their magnetic properties. Depending on the thermal treatment cobalt substituted compounds can be synthesized either in the $TbCu_7$ (disordered) or in the Th_2Zn_{17} (ordered) structure type. Rietveld refinement of the number of transition metal dumbbells replacing rare earth atoms from synchrotron powder diffraction data shows that the $TbCu_7$ disordered structure has the same composition as the ordered one (transition metal to rare earth ratio equal to 8.5). Then cobalt site occupancies have been determined in both structures using synchrotron resonant (anomalous) diffraction. Cobalt is found to be absent from the dumbbell sites. The diffraction results are confirmed by Mössbauer spectroscopy.

Introduction

Today's environment friendly technologies and applications require the development of high-performance permanent magnets with high transition temperatures (T_c) and high specific energy (BH_{max}). In this context, there is a growing interest in nanostructured and highly anisotropic intermetallics based on rare earths (R) and transition metals (T). R_2Fe_{17} compounds have proven to be good candidates for such purpose, especially for their relatively low rare-earth content. Their original magnetic properties are related to the presence of Fe–Fe atom pairs (dumbbells) (1). However, they present a relatively low Curie temperature (T_c < 400K) and exhibit only planar magnetic anisotropy.

Improvement occurs through different mechanisms: electronic and magnetovolumic effects, and modifications of the dumbbells in the material. For Sm_2Fe_{17} based systems, on the one hand, the substitution of Fe by Ga, Si or Mo has a positive impact on the properties (2-4). On the other hand, in the case of Nd_2Fe_{17}, a recent work showed that the magnetic properties can be greatly improved by the substitution of Fe by Co (5).

Furthermore, on the route to Sm_2Fe_{17} synthesis, if the annealing temperature is lower than 800°C, an out-of-equilibrium (metastable) hexagonal phase ($TbCu_7$ prototype, *P*6/*mmm*) is obtained. This hexagonal phase often presents improved magnetic properties compared to the high temperature ordered phase thanks to a slightly improved anisotropy (6-8). The $TbCu_7$ model (*P*6/*mmm*) has been originally proposed by Buschow and van der Goot to account for the non-stoichiometry on the transition metal rich side in $CaCu_5$-type compounds (9). It is accommodated by a random (disordered) replacement of several rare-earth atoms in position 1*a* by transition metal dumbbells oriented along the *c* axis (position 2*e*). Correlatively, a displacement of the transition metal atoms in position 2*c* to the position 6*l* around the missing rare-earth atom is also observed. Transition metals in position 3*g* are unchanged. Note that the name $TbCu_7$ is the name of the prototype and that it does not intimate the composition

because of the disorder. In this structure, the transition metal to rare earth ratio *T*/*R* is not fixed and can change to a large extent (see below).

When the low temperature phase is heated at higher temperature, it evolves towards a rhombohedral phase (Th_2Zn_{17} prototype, $R\bar{3}m$) which is an ordered variant of the $TbCu_7$ structure in which the dumbbells are placed in a staircase pattern, replacing every third rare earth atom. The two structures are shown in Figure 1. The rare-earth atoms in position 1*a* in space group *P*6/*mmm* are in position 6*c* in $R\bar{3}m$. For the transition metals, the correspondence is as follows: 2*e* replaced by 6*c*, 3*g* by 9*d* and 18*h* (split position) and 6*l* by 18*f*.

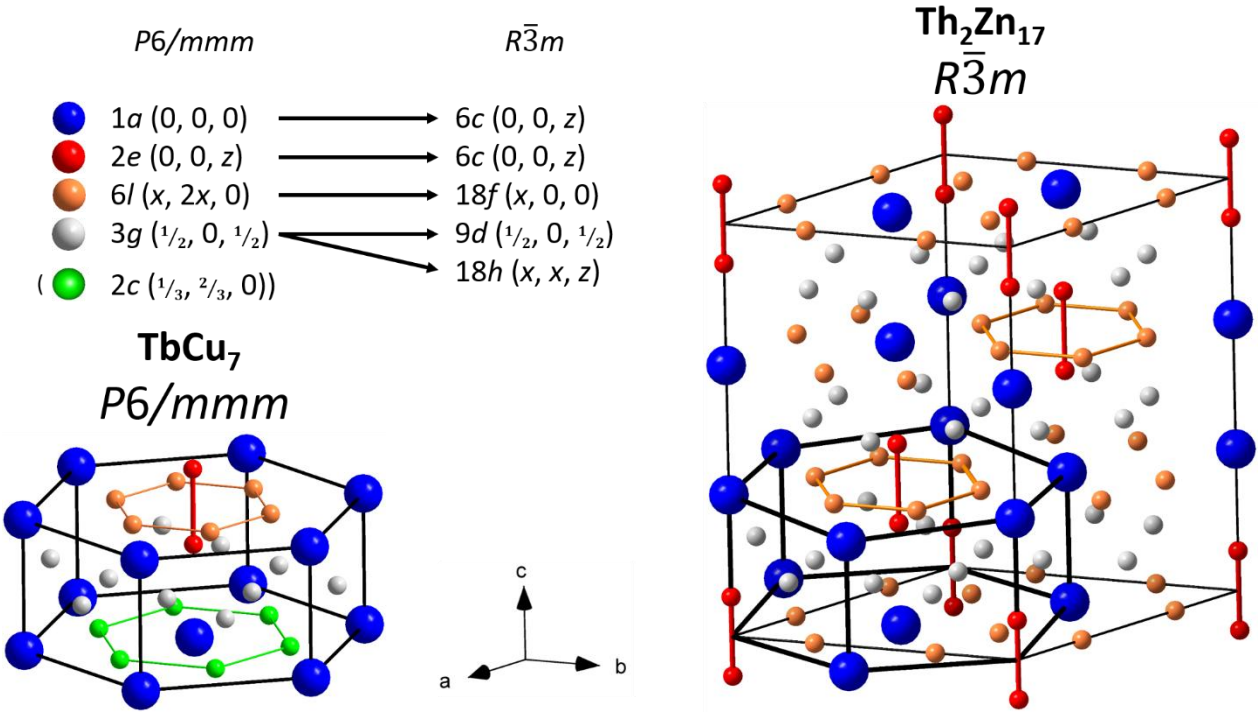

Figure 1. Th_2Zn_{17} and $TbCu_7$ crystal structures. Note that the position 2*c* in green is not occupied in our case.

It is very important to determine on which site, and in which amount, the substituting element locates for subsequent theoretical considerations, such as exchange coupling calculations using the Heisenberg model adopting realistic exchange parameters obtained from first principles, and in order to understand the original magnetic properties of these systems.

Site occupancies have already been determined in these structures in several systems. In $Sm_2Fe_{17-x}M_x$ (*M* = Ga, Si) systems with Th_2Zn_{17} type, the preferred substitution site of Fe is 18*h* (3). In other similar cases however (*M* = Zr, Cr, Mo), the preferred substitution site is 6*c* (4, 10). Several structural studies were also done on $Nd_2Fe_{17-x}Co_x$ giving mixed results between 18*h* and 9*d* as site occupancies for Co (5, 11, 12).

Furthermore, previous works involving X-ray studies on compounds with the $TbCu_7$ prototype such as metastable $SmFe_{9-y}Ga_y$ and $SmFe_{9-y}Si_y$ concluded in the substitution of Fe on the 3*g* site (6, 7).

In the case of Co–Fe–Sm compounds, however, precise determination of the substitution sites has never been done before. For this system, conventional X-ray diffraction cannot be used due to the similar atomic numbers of Co and Fe (Z_{Co}=27, Z_{Fe}=26). Neutron diffraction can neither be used because of the prohibitive absorption of Sm. Therefore, resonant diffraction appears to be the technique of choice. By measuring close to the absorption edge of one of the elements, it allows to contrast Fe and Co and determine by Rietveld refinement of powder diffraction data the site occupancies. Mössbauer spectroscopy is a very interesting complementary technique that allows, on the one hand, to study the influence of Co substitution on the different hyperfine parameters and, on the other hand, to confirm the diffraction results. These two techniques have been used in the present work in order to determine the Co site occupancies in various compounds of formula $Sm_2Fe_{17-x}Co_x$ and in the two structures $TbCu_7$ and Th_2Zn_{17}.

Experimental section

Synthesis

$Sm_2Fe_{17-x}Co_x$ compounds (x = 1, 2, 3 and 4) were prepared by using pure elements (99.9 wt%). The pre-alloys were melted with a slight Sm excess under a high purity argon atmosphere by using an electric arc furnace with a tungsten electrode. To ensure good homogeneity, the obtained ingots were turned over and remelted 5 times.

High energy ball milling for 5 hours under Ar atmosphere in a Fritsch planetary mill was then performed. The obtained nanopowders were wrapped in tantalum foils and vacuum-sealed in silica tubes. The samples were then annealed for 30 min at two different temperatures in order to obtain the intended hexagonal disordered (750°C, in the following called $SmFe_{8.5-x/2}Co_{x/2}$) or the rhombohedral ordered (1200°C, called $Sm_2Fe_{17-x}Co_x$) structures. The thermal treatment was then stopped by quenching the silica tubes in cold water.

Mössbauer

The Mössbauer spectra were obtained using Wissel constant-acceleration spectrometer utilizing a Rh matrix ^{57}Co source. In order to cancel the parabolic distortion, the spectrometer was operating in the mirror-image mode. The calibration of the spectrometer was performed using a standard of α-Fe. The obtained linewidth was equal to 0.26 mm/s. The Mössbauer spectra were refined according to the model discussed below. The estimated errors are at most ± 0.01 mm/s for isomer shifts (δ) and for quadrupole interaction (2ε), and ± 0.1 T for hyperfine fields ($\mu_0 H_{HF}$).

Diffraction

Diffraction measurements were performed on the CRISTAL beamline at SOLEIL synchrotron source at high energy (18470 eV) and selected wavelengths below Fe K-edge (7112 eV). The samples were crushed in agate mortar under inert atmosphere for metastable phases. Due to the relatively high absorption of the samples (μ = 1017 cm^{-1} at 7108 eV, below the Fe K-edge, 302 cm^{-1} at 18470 eV), we mixed the samples powders with 50 wt.% silica and used capillaries of diameter 2*R* = 0.2 mm. This allows to have the best compromise between a reasonable absorption and a decent signal. We recorded the diagrams in Debye-Scherrer geometry, with rotating capillaries, using a detection system made of 9 linear Mythen modules covering a 50° 2θ circle arc. at a distance of 720 mm from the sample. This allowed the obtention of high quality diagrams for all samples at all energies. Silicon powder was measured at all energies in order to refine the wavelength.

The energy was selected using a Si111 monochromator. Prior to diffraction measurements close to the absorption edge, we systematically estimated the average absorption through the capillaries in transmission before edge, and recorded XANES spectra in fluorescence mode (7097-7197 eV energy range, 1 eV resolution), using a SDD Rontec detector, in order to check the Fe K-edge position. A 7 μm Fe foil was used as reference. For XANES spectra, normalization and self-absorption correction were performed using MAX-Cherokee and MAX-Absorbix (13). The edge was defined as the energy of the first maximum of absorption derivative.

Depending on the sample, the measurement in resonant conditions was done either at 7, 8 or 9 eV below the edge. The dispersion coefficients f' and f'' were obtained from Sasaki's tables (14) who used Cromer and Liberman method (15, 16). It was not possible to use calculated f' from the XANES signal and Kramers-Krönig relationship because the energy range that could be accessed was too limited. Towards lower energy, further measurements would have needed a change of the undulator harmonic and at higher energy, we were limited by the presence of Sm L_{II} edge (7312 eV). This is the reason why the measurement was not done too close to the edge, so we could safely use the calculated theoretical

values. The *f'* values obtained are between -6.56 and -6.84 e^- for Fe and -2.3 e^- for Co warranting a sufficient contrast between the two elements.

The data have been analyzed using the Rietveld method using Fullprof (17, 18). The secondary phases detected in each sample have been considered. The line shape was pseudo-Voigt. The internal coordinates and an overall *B* displacement parameter were refined. The site occupancies were refined as follows. For the Th_2Zn_{17} phase, the pattern at low energy is sufficient to solve the multi-site occupancy problem. Each transition metal site was considered as fully occupied by a mixing of Fe and Co. The global composition was constrained to the nominal composition, so only the distribution of the substituting element was refined (3 occupancy parameters). The way to constrain the occupancy parameter of the 4^{th} site to match the nominal composition is detailed in Ref. (19).

For the $TbCu_7$ structure, there is an additional complexity in having to refine the number of dumbbells. We can take advantage of the high energy pattern because the resonant effect is not necessary to refine the dumbbell ratio. But, it is impossible to set the constraints in order to make a joint refinement because the presence of dumbbells does not correspond to a simple substitution scheme as in Ref. (19). Therefore, we used the high energy pattern to determine the number of dumbbells, and then fixed this number for the refinement of the low energy pattern which was therefore refined separately using the same composition constraint as mentioned above. This is not a real problem because we do not expect correlation between the two refinements *i.e.* the refinement of dumbbells is independent on the nature of the atom on the dumbbell because at high energy Co and Fe have similar form factors.

It is extremely difficult to estimate the effective absorption of the samples in the capillary especially because it is almost impossible to determine the quantity of material inside the capillary. Measurements of the transmission direct beam through the capillary gave only approximate results because of geometrical aspects. To solve the problem, and in order to obtain reliable values of the displacement

parameters, we calculated the theoretical absorption ratio between high and low energies. Finally, we made the refinements of the high and low energy patterns with the following constraints: keeping the ratio for the effective absorption equal to the theoretical ratio of absorption coefficients and having equal displacement parameters in the two refinements.

Results

XANES results

Figure 2 presents the XANES of all samples. Since it proved almost impossible to get a precise estimation of the capillaries absorbance, it is difficult to assess whether the differences observed between the diagrams are significant or just due to uncertainties in the auto-absorption correction. However, no change in the edge position is observed compared with Fe foil as illustrated by the XANES derivatives. Changes as a function of the structure or as a function of composition are neither observed. The first maximum of the XANES derivative was used to determine the edge position and set at 7112 eV. The exact energies used for the diagrams measured in resonant conditions were determined based on the distance to the edge: -7 eV, -8 eV or -9 eV, depending on the sample. We observed a 1 eV difference in the energies as determined from the edge or from the refinement of silicon diagrams, which is the order of magnitude of the resolution of the XANES spectra. For the refinement of the diagrams recorded in resonant conditions, we therefore used the wavelength determined by the silicon refinement, and f' and f'' values based on the edge position.

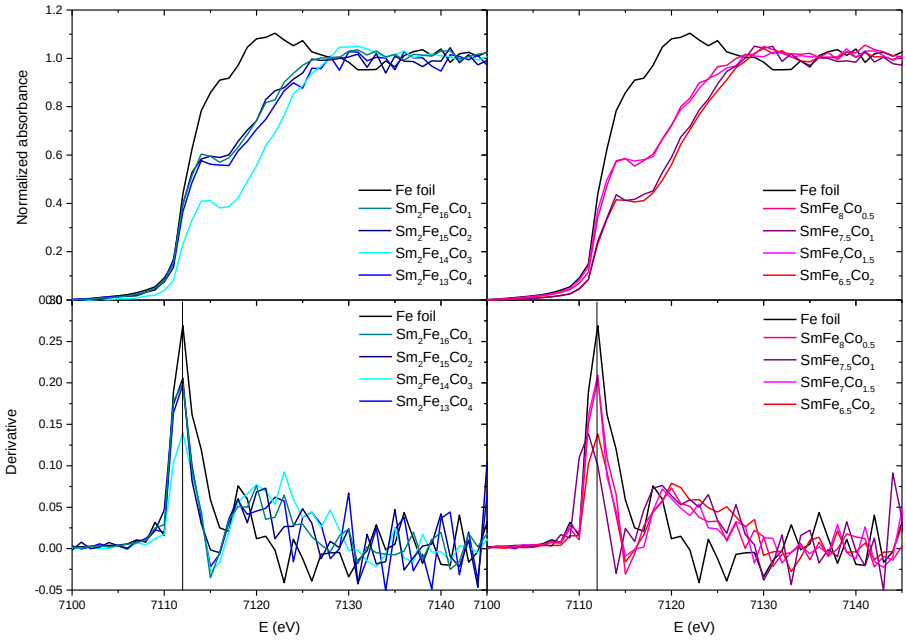

Figure 2. Normalized absorption and first derivative of $Sm_2Fe_{17-x}Co_x$ and $SmFe_{8.5-x/2}Co_{x/2}$ series.

Diffraction results

The phase identification was made from the high energy patterns. The analysis confirmed the presence of the ordered Th_2Zn_{17} phase in the samples prepared at high temperature (1200°C, $Sm_2Fe_{17-x}Co_x$ series) and of the disordered $TbCu_7$ phase in the samples prepared at low temperature (750°C, $SmFe_{8.5-x/2}Co_{x/2}$ series). Secondary phases were always present. Most frequently found are Sm oxides (SmO, SmO_2 and Sm_2O_3 with NaCl, CaF_2 and $(Mn_{0.5}Fe_{0.5})_2O_3$ types) unavoidable with the preparation technique, unreacted α-Fe and other Sm–Fe intermetallic compounds ($SmFe_3$ and Sm_2Fe_{17} with $PuNi_3$ and Th_2Zn_{17} types). They were considered in the refinement. The quantification given in the following is only indicative.

The R/T ratio in the Th_2Zn_{17} phase is fixed by the crystal structure to 2/17. Non-stoichiometry has not been reported in this ordered phase. This ratio corresponds also to the nominal composition of our samples. On the other hand, the cobalt to iron ratio is fixed by the nominal composition.

The situation is less obvious for the disordered phase because, due to the disorder, the R/T ratio cannot be guessed from the structure. However, it can be obtained from the structural refinement. This refinement has been done on the high energy pattern. The refined composition, according to Buschow's model (9, 20) is as follows:

$$\mathrm{Sm}_{1-s}^{1a}(\mathrm{Fe,Co})_{2s}^{2e}(\mathrm{Fe,Co})_{2-6s}^{2c}(\mathrm{Fe,Co})_{6s}^{6l}(\mathrm{Fe,Co})_{3}^{3g} \qquad (1)$$

This model derives from the $CaCu_5$ model in which sites 1*a*, 2*c* and 3*g* are completely occupied. Rare earth atoms in position 1*a* are replaced by dumbbells of transition metals in position 2*e*. Correlatively a corresponding amount of the transition metals in position 2*c* is displaced towards the missing rare earth atom (position 6*l*). It has been shown by total scattering experiments that this displacement is indeed locally correlated (21). The parameter *s* can change from 0 to 1/3, in this model, able to describe compositions from RT_5, corresponding to the $CaCu_5$ structure, up to $RT_{8.5}$ with no atom in position 2*c*. Note that higher T/R compositions can be obtained with different models (22).

Within this scheme only one parameter, *s*, was refined. In each case, the refinement gives a value of *s* extremely close to 1/3. The convergence of this parameter towards this value, without any constraint, is remarkable. This ratio corresponds to the maximum number of dumbbells that can be obtained in the above model. Site 2*c* (in green in Fig. 1) which is completely vacant has therefore not been considered in the subsequent refinements. This result is also important because it indicates that the composition is $R_{0.666}T_{5.666}$, *i.e.* corresponding exactly to a ratio R/T=2/17. This indicates that the two phases with the structures Th_2Zn_{17} and $TbCu_7$ have indeed the very same compositions and transform one into each

other as a function of the temperature treatment. As indicated in the experimental section, the number of dumbbells has been fixed in the subsequent refinement of the site occupancies.

To summarize, the lattice parameters, *B*, atomic positions and number of dumbbells for the $SmFe_{8.5-x/2}Co_{x/2}$ series, have been refined from the high energy pattern, while the cobalt to iron substitution has been obtained from the low energy pattern using the resonant effect. The complete results can be found in Tables 1 and 2. Figures 3 and 4 show examples of the refinements for the two structures and at the two different energies.

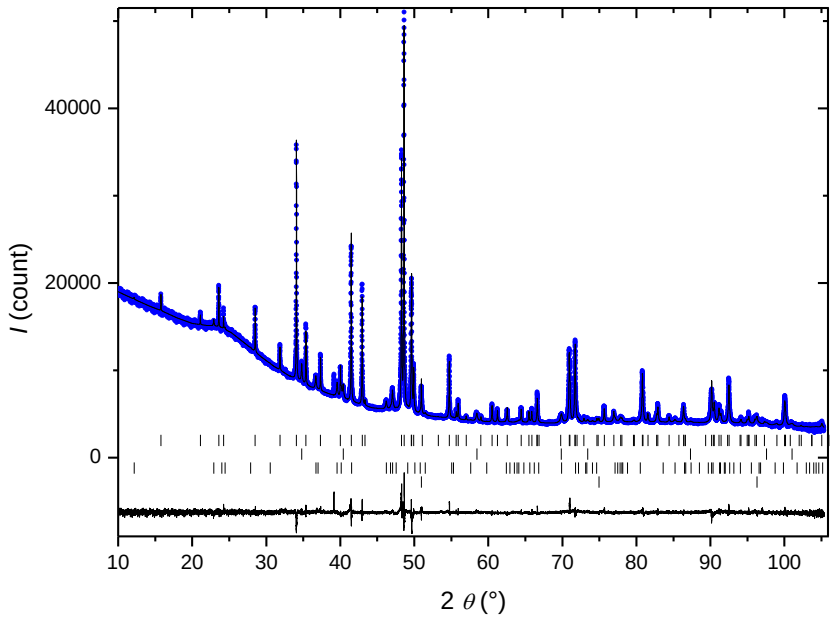

Figure 3. Rietveld plot of $Sm_2Fe_{13}Co_4$ (*x*=4) at 7104 eV (8 eV below the Fe edge). Experimental (points), calculated (line) and difference (line below) patterns are shown. The markers show the positions of (from top to bottom) Th_2Zn_{17} phase, SmO, $SmFe_3$, α-Fe.

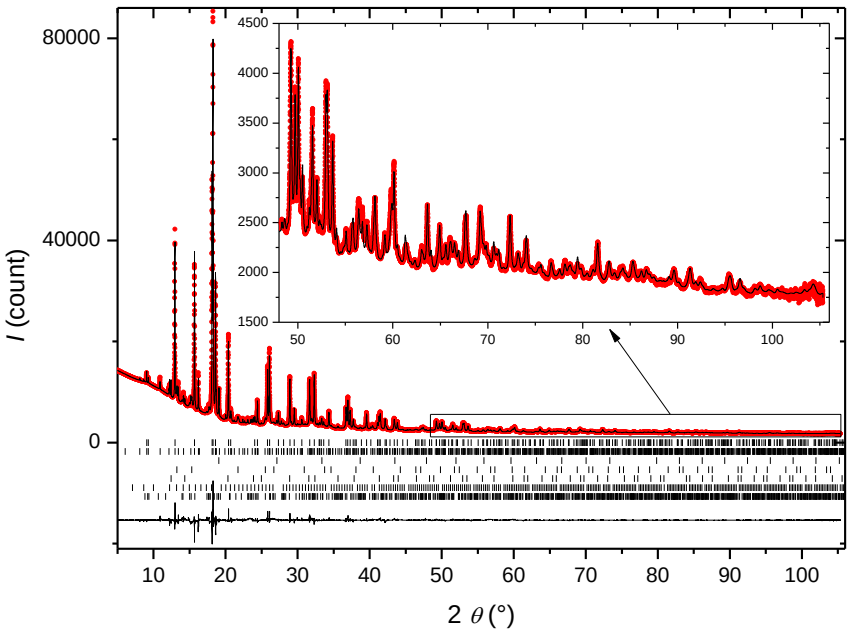

Figure 4. Rietveld plot of $SmFe_7Co_{1.5}$ (*x*=3) at 18470 eV. Experimental (points), calculated (line) and difference (line below) patterns are shown. The markers show the positions of (from top to bottom) $TbCu_7$ phase, Th_2Zn_{17} phase, α-Fe, SmO, SmO_2, Sm_2O_3, $SmFe_3$.

Composition	$Sm_2Fe_{16}Co_1$	$Sm_2Fe_{15}Co_2$	$Sm_2Fe_{14}Co_3$	$Sm_2Fe_{13}Co_4$
x	1	2	3	4
Secondary phases (wt.%)	SmO (4%) Sm_2O_3 (10%) α-Fe (0.3%)	SmO (3%) monoclinic-Sm_2O_3 (4%) $SmFe_3$ (4%)	SmO (2%)	SmO (2%) $SmFe_3$ (9%)
a (Å)	8.5518(1)	8.5445(1)	8.5408(1)	8.5320(1)
c (Å)	12.4574(2)	12.4696(2)	12.4716(2)	12.4765(2)
x_{18h}	0.5012(1)	0.5014(1)	0.5011(1)	0.5010(2)
z_{18h}	0.1570(2)	0.1569(2)	0.1575(2)	0.1572(2)
x_{18f}	0.2911(2)	0.2922(2)	0.2922(2)	0.2923(3)
z_{6c} (Fe,Co)	0.0964(2)	0.0962(2)	0.0959(2)	0.0956(3)
z_{6c} (Sm)	0.3425(1)	0.3425(1)	0.3420(1)	0.3424(1)
Co in 18*h* (atom)	2.0(4)	2.7(7)	3.7(2)	5.8(3)
Co in 18*f* (atom)	0.2(4)	1.3(7)	3.0(2)	2.3(3)
Co in 9*d* (atom)	1.2(3)	1.6(6)	2.2(2)	3.0(3)
Co in 6*c* (atom)	-0.4(4)	0.6(4)	0.0(2)	0.9(3)
B ($Å^2$)	0.415(6)	0.473(7)	0.513(8)	0.506(9)
R_B (%) HE	2.6	3.6	6.5	4.2
R_B (%) LE	5.4	7.0	8.2	7.3

Table 1. Results for the $Sm_2Fe_{17-x}Co_x$ samples, space group *R*-3*m*. Estimated standard deviations calculated by Fullprof (in brackets referring to the last digit) have been multiplied by the Bérar parameter (between 3 and 7). Bragg *R* factors are given for the high (HE) and low (LE) energy pattern refinements.

Composition	$SmFe_8Co_{0.5}$	$SmFe_{7.5}Co_1$	$SmFe_7Co_{1.5}$	$SmFe_{6.5}Co_2$
x	1	2	3	4
Secondary phases	α-Fe (4%) SmO (4%) SmO_2 (5%) Sm_2O_3 (6%) $SmFe_3$ (7%)	α-Fe (4%) SmO (4%) SmO_2 (2%) Sm_2O_3 (9%) $SmFe_3$ (3%)	α-Fe (3%) SmO (3%) SmO_2 (1%) Sm_2O_3 (1%) Sm_2Fe_{17} (35%) $SmFe_3$ (3%)	α-Fe (4%) SmO (4%) SmO_2 (3%) Sm_2Fe_{17} (28%) $SmFe_3$ (8%)
a (Å)	4.9296(4)	4.9266(4)	4.9292(4)	4.9251(5)
c (Å)	4.1633(4)	4.1655(4)	4.1589(4)	4.1543(5)
x_{6l}	0.292(1)	0.292(1)	0.291(2)	0.291(2)
z_{2e}	0.290(3)	0.293(3)	0.291(4)	0.291(5)
s	0.338(4)	0.336(5)	0.335(9)	0.335(10)
Co in 3*g* (atom)	0.35(3)	0.51(3)	0.79(3)	1.04(4)
Co in 6*l* (atom)	0.02(4)	0.11(3)	0.21(3)	0.33(4)
Co in 2*e* (atom)	-0.03(3)	0.04(3)	-0.01(3)	-0.04(4)
B ($Å^2$)	0.45(2)	0.51(2)	0.53(2)	0.51(3)
R_B (%) HE	4.8	5.3	4.8	5.3
R_B (%) LE	5.0	5.8	3.2	6.8

Table 2. Results for the $SmFe_{8.5-x/2}Co_{x/2}$ samples, space group *P*6/*mmm*. Estimated standard deviations calculated by Fullprof (in brackets referring to the last digit) have been multiplied by the Bérar parameter (between 3 and 10). Bragg R factors are given for the high (HE) and low (LE) energy pattern refinements.

The lattice parameters of the $Sm_2Fe_{17-x}Co_x$ samples phase depend regularly on the Co composition with an increase of the *c*/*a* ratio as a function of *x* (Figure 5) which is not the case for the $SmFe_{8.5-x/2}Co_{x/2}$ samples (Figure 6). It reveals that the Co substitution expands the lattice along the *c* axis only in the case of ordered dumbbels, whereas the effect is negligible in the disordered structure. The *B* parameter dependence as a function of composition is shown in Figure 7 for the two phases. The observed increase can be related to the higher static displacement caused by the substitution. On the other hand, only slight variation of atomic coordinates is observed with composition (not shown).

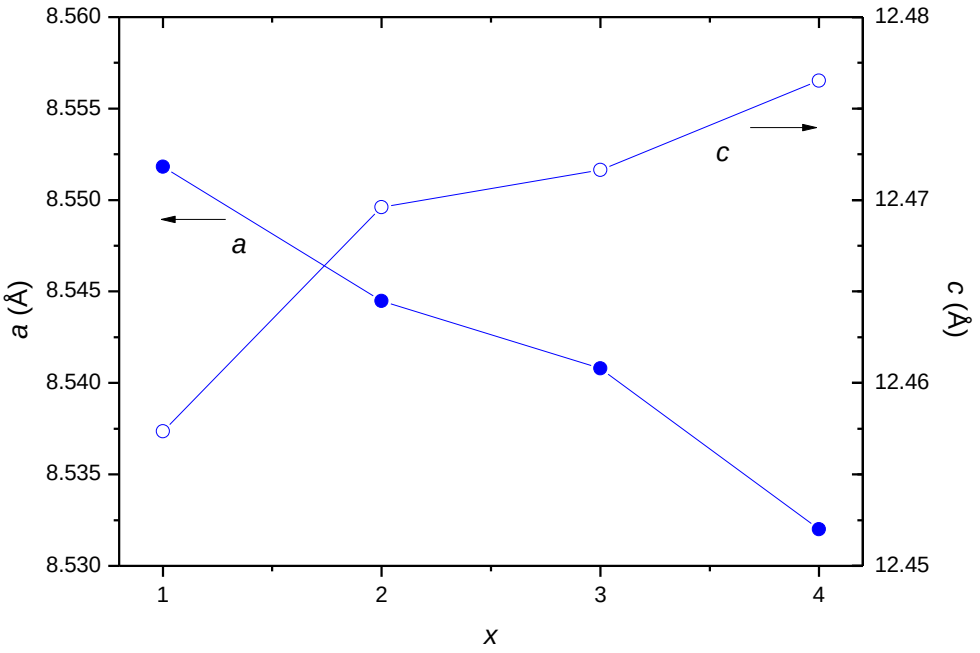

Figure 5. lattice parameters of the $Sm_2Fe_{17-x}Co_x$ series as a function of *x* (error bars are smaller than the symbols).

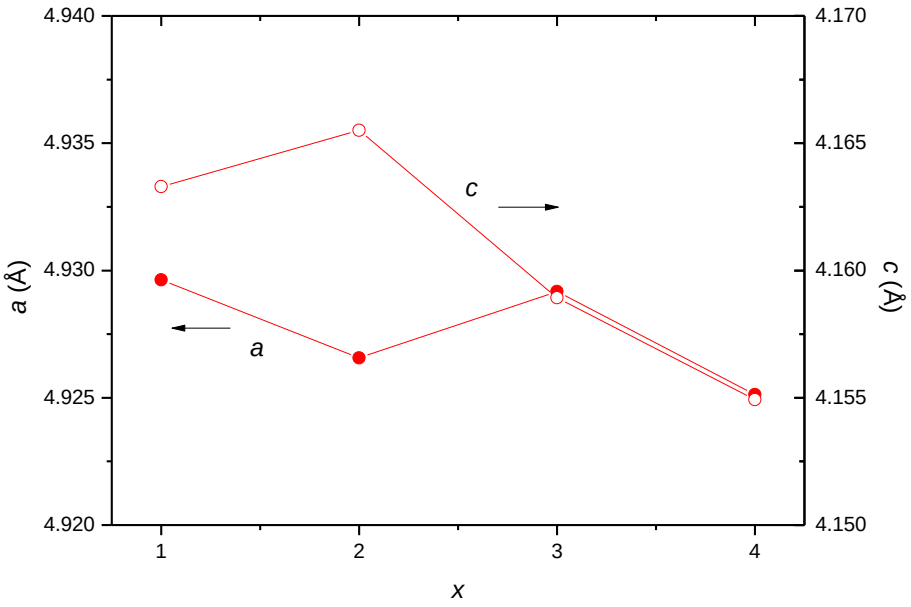

Figure 6. lattice parameters of the $SmFe_{8.5-x/2}Co_{x/2}$ series as a function of *x* (error bars are smaller than the symbols).

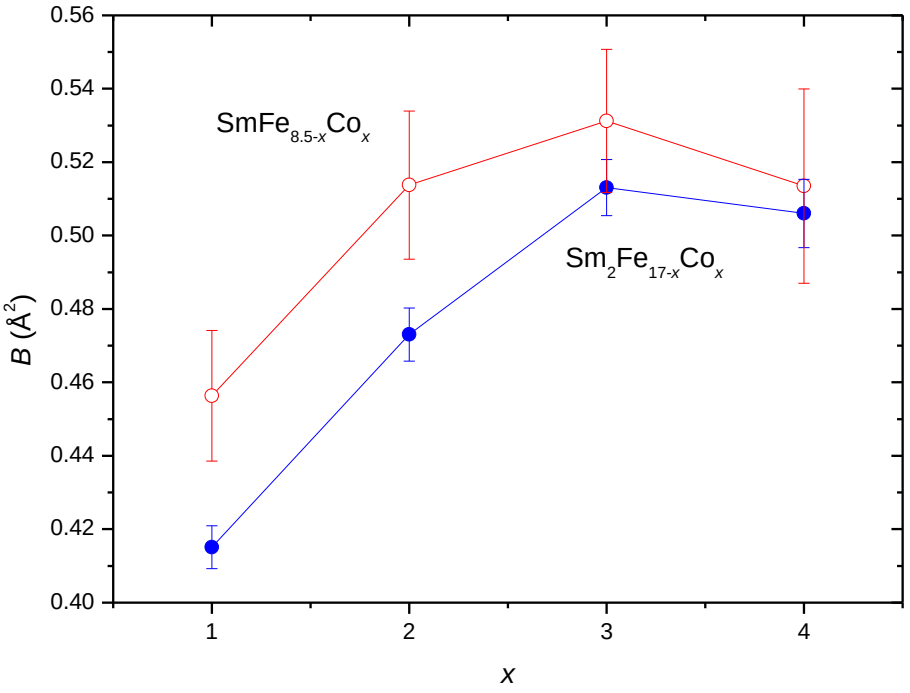

Figure 7. displacement parameters as a function of *x* for $Sm_2Fe_{17-x}Co_x$ and $SmFe_{8.5-x/2}Co_{x/2}$

The occupancy parameters are plotted for $Sm_2Fe_{17-x}Co_x$ (Figure 8) and $SmFe_{8.5-x/2}Co_{x/2}$ series (Figure 9) phases. Higher estimated standard deviations are observed for the ordered phase which are related to its higher structural complexity. We can nevertheless observe clear trends in the occupancy parameters with a significantly higher cobalt occupancy in site 18*h* and an almost null Co occupancy in site 6*c*. For the disordered phase, the partition of cobalt is also very different among the different sites with a clear preference for site 3*g* and no occupancy in the dumbbell position in site 2*e*.

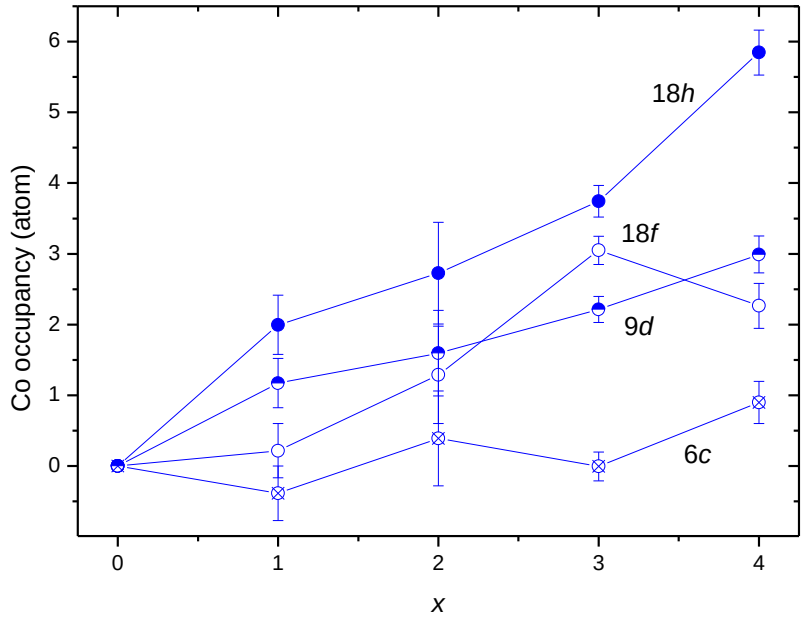

Figure 8. Cobalt site occupancies (in atom per site) for the $Sm_2Fe_{17-x}Co_x$ series.

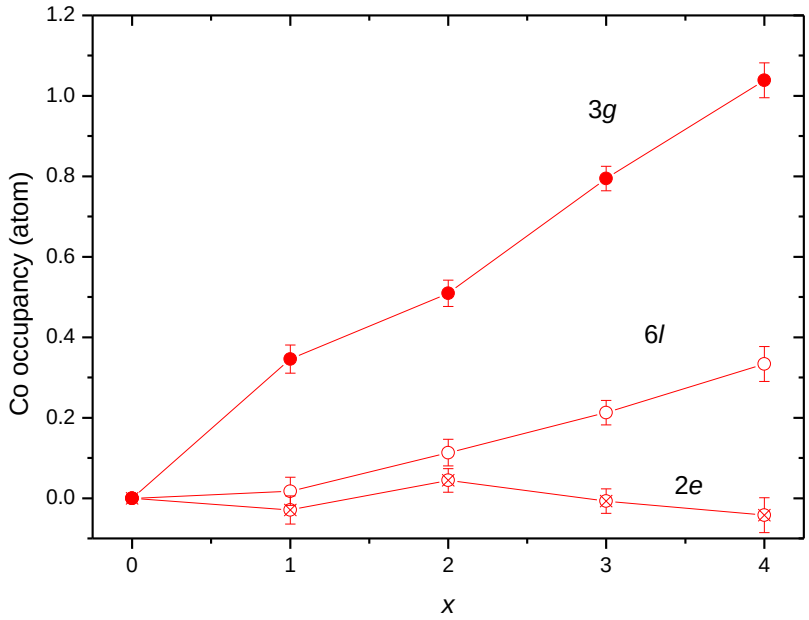

Figure 9. Cobalt site occupancies (in atom per site) for the $SmFe_{8.5-x/2}Co_{x/2}$ series.

Mössbauer results

Mössbauer spectrometry is the recoil-free emission and resonant absorption of γ-rays in solids, *i.e.* γ -ray emission and absorption without the loss of energy to the lattice. The Mössbauer spectra of the $Sm_2Fe_{17-x}Co_x$ and $SmFe_{8.5-x/2}Co_{x/2}$ series are complex. The solution chosen for their analysis must correspond to a model justified by experimental approaches resulting from other techniques or based on relevant theoretical considerations. The reliability of the proposed model for the interpretation of the experimental spectra must be demonstrated by the monotonic evolution of the hyperfine parameters, isomer shift (δ) and hyperfine field ($\mu_0 H_{HF}$). The simulation is based on several criteria outlined below:

- The environments of Fe atoms have been established based on a multinomial distribution law as a function of the distribution of atoms, obtained after the crystallographic study.
- The assignment of the hyperfine parameters to the different inequivalent crystallographic sites is determined by the correlation between the isomer shift and the volume of the Wigner-Seitz cells (WSCV). We have used the crystallographic characteristics (unit cell parameters and atomic positions) for the calculation of the WSCV.
- The assumption of relative intensities of the sextuplet lines in the 3:2:1 ratio of a randomly oriented powder system was considered due to the absence of crystallographic texture.
- Lamb-Mössbauer absorption factors were considered equal for all sites.

In Figure 10, the experimental spectra for $Sm_2Fe_{15}Co_2$ and $SmFe_{7.5}Co_1$ at room temperature are presented. One can notice a shoulder in the region corresponding to the velocities +5.5 mm/s for $Sm_2Fe_{15}Co_2$ and -5.5 mm/s for $SmFe_{7.5}Co_1$, which is attributable to the Fe-Fe dumbbells at sites 6*c* and 2*e*, respectively. Further refinement shows that the abundance of these sites corresponds to a total occupation by iron of site 6*c* for $Sm_2Fe_{15}Co_2$ and of site 2*e* for $SmFe_{7.5}Co_1$. This result agrees with our

finding that cobalt neither occupies sites *6c* nor 2*e*. We will explain the results obtained from the structural refinement, that cobalt is preferentially distributed among sites 18*h* and 3*g*.

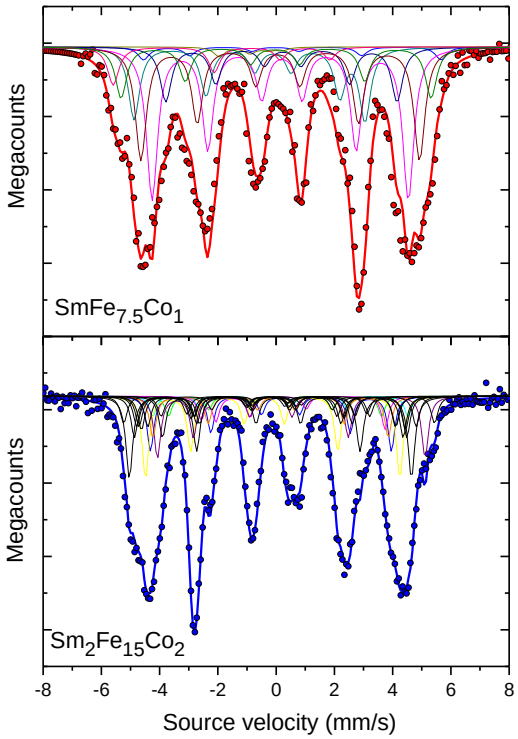

Figure 10. Room temperature Mössbauer spectra for $Sm_2Fe_{15}Co_1$ and $SmFe_{7.5}Co_1$ compounds. The thick lines and the symbols correspond to the calculated and experimental spectra, respectively. The different sextets used in the refinement are presented by colored thin lines.

	<6*c*>	<9*d*>	<18*f*>	<18*h*>	wt. ave.
$\mu_0 H_{HF}$ (T)	31.5	28.2	26.4	25.3	27.3
δ (mm/s)	0.16	-0.01	-0.06	0.02	0.01
2ε (mm/s)	0.17	0.03	-0.10	0.01	-0.01
WSCV (A^3)	13.1	11.6	11.9	12.4	12.2

Table 3. Mössbauer hyperfine parameters for $Sm_2Fe_{15}Co_2$ sample. $\mu_0 H_{HF}$ is the hyperfine field, δ is the isomer shift, 2ε is the quadrupole interaction and WSCV is the Wigner-Seitz cell volume.

	<2*e*>	<3*g*>	<6*l*>	wt. ave.
$\mu_0 H_{HF}$ (T)	30.0	25.7	26.3	26.8
δ (mm/s)	0.13	0.02	-0.02	0.04
2ε (mm/s)	0.03	-0.02	-0.10	-0.03
WSCV (A^3)	18.0	12.8	12.2	14.1

Table 4. Mössbauer hyperfine parameters for $SmFe_{7.5}Co_1$ sample. $\mu_0 H_{HF}$ is the hyperfine field, δ is the isomer shift, 2ε is the quadrupole interaction and WSCV is the Wigner-Seitz cell volume.

A single line width of 0.28 mm/s has been imposed to limit the number of sites needed to fit Mössbauer spectra. We neglected theoretical abundances lower than 1.5% for $Sm_2Fe_{17-x}Co_x$ and 2% for $SmFe_{8.5-x/2}Co_{x/2}$.

During the refinement of the hyperfine parameters, the abundances of the different sites were considered as fixed, while the hyperfine parameters δ, *H* and 2ε were released.

In the first step of the refinement, the assignment of the hyperfine field to all the subspectra associated with a particular crystallographic site was based on the physical fact that the highest hyperfine field

belonged to site *6c* (*2e*) and the lowest to site *9d* (3*g*) according to their respective theoretical abundances. At this stage, no distinction was made between sites 18*f* and 18*h*. In the second step, a mean value of δ was assigned to each hyperfield taking into account the correlation between δ and WSCV volume. Then, the refinement was performed with all free parameters except abundance and finally, in the last step, we freed all hyperfine parameters. The sets of hyperfine parameters resulting from such a refinement are given in Table 3 and 4 for *x*=2 as an example.

Figures 11 and 12 show the evolution of the isomer shift of each of the sites as a function of *x*.

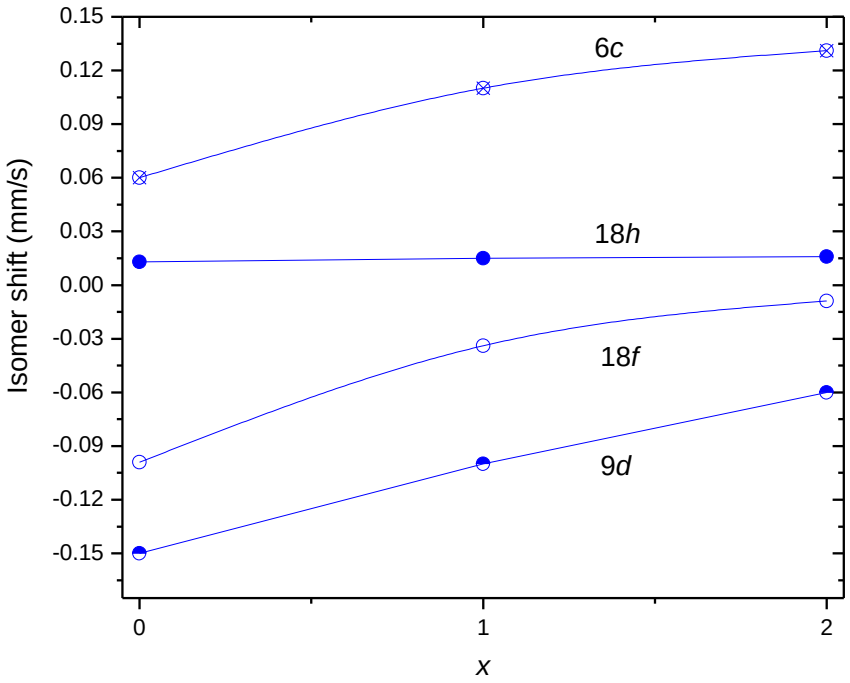

Figure 11. isomer shift for the $Sm_2Fe_{17-x}Co_x$ series.

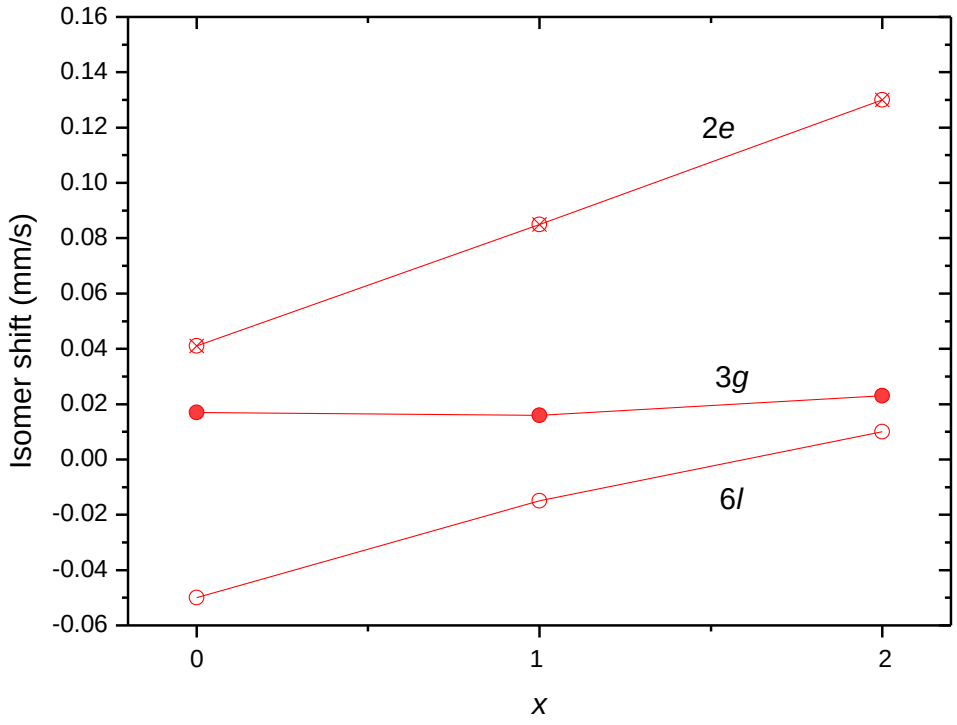

Figure 12. Isomer shift for the $SmFe_{8.5-x/2}Co_{x/2}$ series.

Discussion

Due to the planar orientation of the magnetization in both phases for sites 9*d*, 18*h* and 18*f* in space group $R\bar{3}m$, and 3*g* and 6*l* in space group *P*6/*mmm*, the angle between the hyperfine field and the electric field gradient is not zero. Each of these sites will be decomposed into two non-equivalent magnetic sites with relative abundances equal to 2:1, as a consequence, during the refinement of the Mössbauer spectra we have used several sextets relating to the different magnetic sub-sites.

The isomer shift δ of an individual site, can be predicted qualitatively from the perturbation brought by Co 3*d* electrons at the *s* electron density to the iron nuclei of the site considered. Indeed, according to

the expression of the isomer shift δ is a function of the electron density *s* at the nucleus multiplied by a nuclear factor $\left(\frac{\Delta R}{R}\right)$, negative in the case of iron:

$$\delta = \frac{1}{5\varepsilon_0} Ze^2 \left(\frac{\Delta R}{R}\right) [|\psi_s(0)_{abs}|^2 - |\psi_s(0)_{source}|^2] \quad (2)$$

Where $|\psi_s(0)_{abs}|^2$ is the non-relativistic Schrödinger wave function (at *r* = 0), and ΔR is the change in nuclear radius. The larger $|\psi_s(0)_{abs}|^2$ is, the smaller δ is and vice versa. The result is that the Co *d* electrons that fill the Fe *d* band will shield the *4s* electrons of Fe atoms. As a result, the density $|\psi_s(0)_{abs}|^2$ at the iron core will be reduced, so the isomer shift will increase as a function of the Co content. Furthermore, for a given value of Co content, the correlation between δ and WSCV volume shown above must be considered, the greater the WSCV volume, the greater δ (23, 24).

Whatever the Co content, the observed sequence is δ9*d* < δ18*f* < δ18*h* < δ6*c* for $Sm_2Fe_{17-x}Co_x$ and δ6*l* < δ3*g* < δ2*e* for $SmFe_{8.5-x/2}Co_{x/2}$, which corresponds to the evolution of WSCV.

The increase of the isomer shift for 6*c*, 18*f* and 9*d* (2*e* and 6*l*), with Co content, is the consequence of the shielding of Fe *4s* electrons by the additional Co 3*d* electrons. As explained above, the evolution of the isomer shift for the different crystallographic sites with cobalt content is the consequence of the shielding of Fe *4s* electrons by the additional cobalt 3*d* electrons. δ6*c*, δ18*f* and δ9*d* (δ2*e* and δ6*l*), show an increase with cobalt substitution, whereas δ18*h* (δ3*g*) remains quasi-constant. This result can be understood in terms of preferential cobalt atom occupation. For the hexagonal $TbCu_7$ structure, the 2*e* and 6*l* Fe atoms have six adjacent 3*g* neighbors while the 3*g* atom site has only four. The 3*g* atoms with the fewest 3*g* neighbors are the least affected by cobalt substitution and their *s* electron charge density is then quasi modified. Concerning the rhombohedral Th_2Zn_{17} structure, the 6*c*, 9*d,* and 18*f* sites have three, four and four adjacent 18*h* neighbors whereas the 18*h* iron site has only two. The 18*h* atoms with

the smallest 18*h* neighbors are the least affected by cobalt substitution and consequently δ18*h* is less modified.

The structure model obtained from diffraction was mandatory to refine the Mössbauer results because of the high complexity of the spectra. However, the good quality of the Mössbauer refinements and the monotonic variation of the hyperfine field (not shown) and isomeric shift (Figures 11 and 12) testifies, in turn, for the relevance and accuracy of the structure model.

The refinement of the high energy diffraction patterns of $SmFe_{8.5-x/2}Co_{x/2}$ samples, gives a *s* value always converging exactly to 0.333 which is the maximum number of dumbbells in a disordered model giving an explanation why the stable phase actually orders when activated by temperature without any composition change. The refinement of this parameter with such an accuracy to this particular value has not been reported previously, as far as we are aware.

The two crystal structures are related, the stable Th_2Zn_{17} derives from the disordered $TbCu_7$ structure by ordering of the dumbbells. Each site in the Th_2Zn_{17} therefore derives from a position in the $TbCu_7$ structure *i.e.* sites 18*h* and 9*d* derive from site 3*g*, 18 *f* from 6*l* and 6*c* from 2*e*. Therefore, similar cobalt site occupancies are expected. From a comparison of Figures 8 and 9, it is shown that it is the case (maximum occupancy for sites 18*h* and 3*g*, null occupancy for the dumbbell position 6*c* and 2*e*). It is remarkable that the site occupancies (expressed in percentage not in atom per site) are found identical in the two sites 9*d* and 18*h* originating from the symmetry splitting of site 3*g* in space group *P*6/*mmm.* .

Concerning the Th_2Zn_{17} type, the results found for $Sm_2Fe_{17-x}Co_x$ compounds are in good agreement with previous works on the same system (25) and with literature on other systems (3-5, 10-12, 26). Regarding the disordered $SmFe_{8.5-x/2}Co_{x/2}$ series, the resulting preference of cobalt for site 3*g* is also shared by gallium and silicon atoms with similar structures [6,7] even though gallium and silicon atoms have slightly different radii compared to that of cobalt. The main reason explaining the preferred site occupancies of

site 3*g* by the larger atoms (here Co) in the $TbCu_7$ structure and of sites 9*d* and 18*h* in the Th_2Zn_{17} structure seems to be the larger size of this site.

The precise determination of the cobalt site in the $Sm_2Fe_{17-x}Co_x$ and $SmFe_{8.5-x/2}Co_{x/2}$ series is necessary for the understanding of the intrinsic magnetic properties (*e.g.* exchange interaction, Curie temperature) as well as for the calculation of the electronic structure by first-principles approach. This step is essential before optimizing the microstructure in order to obtain the optimal energy product (BH)max for hard magnets. The correlation between Co position and magnetic properties will be done in an upcoming paper.

Conclusion

We have refined from resonant diffraction data obtained at the Fe K-edge the distribution of substituting Co in ordered and disordered Sm_2Fe_{17} compounds. We found, from the structural refinement, that the two phases have the same composition for each Co amount. The Co site occupancies between the two phases follow the site equivalence between the two structures. The results are also in perfect agreement with both our own Mössbauer spectroscopy measurements on this system and other results previously obtained on other systems. This new and relevant structural analysis, of the two phases, will allow us to make DFT calculations under optimal conditions. This will give us the magnetic moment for each inequivalent crystallographic site.

References

(1) Givord, D.; Lemaire, R., Magnetic transition and anomalous thermal-expansion in R_2Fe_{17} compounds. *IEEE Transactions on Magnetics* **1974,** MA10 109-113.

(2) Kubis, M.; Eckert, D.; Gebel, B.; Müller, K.-H.; Schultz, L., Intrinsic magnetic properties of $Sm_2Fe_{17-x}M_xN_y/C_y$ (M=Al, Ga or Si). *J. Magn. Magn. Mater.* **2000,** 217 (1-3), 14-18.

(3) Bessais, L.; Dorolti, E.; Djéga-Mariadassou, C., Correlation between $Sm_2(Fe,Ga)_{17}$ and its precursor $Sm(Fe,Ga)_9$. *J. Appl. Phys.* **2005,** 97 013902.

(4) Bessais, L.; Younsi, K.; Khazzan, S.; Mliki, N., X-ray and intrinsic magnetic properties of nanocrystalline $Sm_2(Fe,M)_{17}$ (M = Si, Ga, Co, Cr, Zr or Mo). *Intermetallics* **2011,** 19 (7), 997-1004.

(5) Bouchaala, N.; Jemmali, M.; Bartoli, T.; Nouri, K.; Hentech, I.; Wahla, S.; Bessais, L.; Ben Salah, A., Influence of Fe-substitution on structural, magnetic and magnetocaloric properties of $Nd_2Fe_{17-x}Co_x$ solid solutions. *J. Solid State Chem.* **2018,** 258 501-508.

(6) Djéga-Mariadassou, C.; Bessais, L.; Nandra, A.; Burzo, E., Crystallographic and magnetic study of metastable nanocrystalline $Sm(Fe,Si)_9$. *Phys. Rev.* **2003,** B68 024406.

(7) Bessais, L.; Dorolti, E.; Djéga-Mariadassou, C., High coercivity in nanocrystalline carbides $Sm(Fe,Ga)_9C$. *Appl. Phys. Lett.* **2005,** 87 192503.

(8) Guetari, R.; Bartoli, T.; Cizmas, C.B.; Mliki, N.; Bessais, L., Structure, magnetic and magnetocaloric properties of new nanocrystalline $(Pr,Dy)Fe_9$ compounds. *J. Alloys Compd.* **2016,** 684 291-298.

(9) Buschow, K.H.J.; van der Goot, A.S., Composition and crystal structure of hexagonal Cu-rich rare earth-copper compounds. *Acta Crystallogr.* **1971,** B27 1085-1088.

(10) Chen, Z.; Hadjipanayis, G.C.; Daniel, M.; Digas, M.; Moukarika, A.; Papaefthymiou, V., Effects of substitutions M on the formation, structure and magnetic properties of $Sm_2Fe_{15}M_2C_2$ (M = V, Cr, Ti, Nb, Zr, Mn and Mo) compounds. *J. Magn. Magn. Mater.* **1998,** 177-181 (2), 1109-1110.

(11) Ryan, D.H.; Altounian, Z.; Liao, L.X.; Ström-Olsen, J.O.; Muir, W.B., Direct determination of cobalt site preferences at infinite dilution in iron-based intermetallic compounds. *J. Appl. Phys.* **1990,** 67 4742.

(12) Liao, L.X.; Ryan, D.H.; Altounian, Z., Mössbauer determination of cobalt substitution in iron-based intermetallics. *J. Appl. Phys.* **1991,** 70 6143.

(13) Michalowicz, A.; Moscovici, J.; Muller-Bouvet, D.; Provost, K., MAX: Multiplatform Applications for XAFS. *Journal of Physics Conference Series* **2009,** 190 012034.

(14) Sasaki, S., Numerical tables of anomalous scattering factors calculated by the Cromer and Liberman method, 1989.

(15) Cromer, D.T.; Liberman, D.A., *J. Chem. Phys.* **1970,** 53 1891-1898.

(16) Cromer, D.T.; Liberman, D.A., *Acta Crystallogr.* **1981,** A37 267-268.

(17) Rodríguez-Carvajal, J., Fullprof: a program for Rietveld refinement and pattern matching analysis. *XV Congress of Int. Union of Crystallography, Satellite Meeting on Powder Diffraction* **1990,** 127.

(18) Rodríguez-Carvajal, J., Recent developments of the program FULLPROF. *Commission on Powder Diffraction, Newsletter* **2001,** (26), 12-19.

(19) Joubert, J.-M.; Cerný, R.; Latroche, M.; Percheron-Guégan, A.; Yvon, K., Site occupancies in $LaNi_5$ three-substituted compound determined by means of multiwavelength X-ray powder diffraction. *J. Appl. Crystallogr.* **1998,** 31 327-332.

(20) Joubert, J.-M.; Cerný, R.; Latroche, M.; Leroy, E.; Guénée, L.; Percheron-Guégan, A.; Yvon, K., A structural study of the homogeneity domain of $LaNi_5$. *J. Solid State Chem.* **2002,** 166 1-6.

(21) Cerny, R.; Filinchuk, Y.; Brühne, S., Local atomic order in the vicinity of Cu_2 dumbbells in $TbCu_7$-type $YCu_{6.576}$ studied by Bragg and total scattering techniques. *Intermetallics* **2009,** 17 818-825.

(22) Bessais, L.; Djéga-Mariadassou, C., Structure and magnetic properties of nanocrystalline $Sm(Fe_{1-x}Co_x)_{11}Ti$ (x<~2). *Phys. Rev.* **2001,** B63 054412.

(23) Forker, M.; Julius, A.; Schulte, M.; Best, D., Mossbauer study of the hyperfine interaction of Fe-57 in $Y_{1-s}Co_{5+2s}$ and related compounds. *Phys. Rev.* **1998,** B57 (18), 11565-11574.

(24) Bessais, L.; Sab, S.; Djéga-Mariadassou, C.; Grenèche, J.-M., Crystallographic and hyperfine parameters of $PrTi(Fe,Co)_{11}$ and their carbides. *Phys. Rev.* **2002,** B66 (5), 054430.

(25) Bessais, L.; Djéga-Mariadassou, C.; Tung, D.K.; Hong, V.V.; Phuc, N.X., A Fe-57 Mossbauer study of nanostructured $Sm_2Fe_{17-x}Co_xC_3$. *J. Alloys Compd.* **2008,** 455 (1-2), 35-41.

(26) Yili Cao; Kun Lin; Zhanning Liu; Jinyu Hu; Chin-Wei Hang; Maxim Avdeev; Quiang Li; Jinxia Deng; Jun Chen; Hongjie Zhang; XIanran Xing, Neutron diffraction study of unusual magnetic behaviors in the $Ho_2Fe_{11}Al_6$ intermetallic compound. *Inorg. Chem.* **2019,** 58 13742-13745.

Synopsis

The cobalt site occupancies in substituted Sm_2Fe_{17} (Th_2Zn_{17}-type) and $SmFe_{8.5}$ ($TbCu_7$-type) have been determined by Rietveld refinement of resonant diffraction data measured at the iron K-edge. Results are compared with Mössbauer spectroscopy measurements.

Table of content graphics